# Fine-scale processes regulate the response of extreme events to global climate change

**Noah S. Diffenbaugh*†, Jeremy S. Pal‡, Robert J. Trapp*, and Filippo Giorgi‡**

*Purdue Climate Change Research Center and Department of Earth and Atmospheric Sciences, Purdue University, 550 Stadium Mall Drive, West Lafayette, IN 47907-5201; and ‡Earth Systems Physics Group, Abdus Salam International Centre for Theoretical Physics, 34014 Trieste, Italy

Edited by Stephen H. Schneider, Stanford University, Stanford, CA, and approved September 11, 2005 (received for review July 17, 2005)

**We find that extreme temperature and precipitation events are likely to respond substantially to anthropogenically enhanced greenhouse forcing and that fine-scale climate system modifiers are likely to play a critical role in the net response. At present, such events impact a wide variety of natural and human systems, and future changes in their frequency and/or magnitude could have dramatic ecological, economic, and sociological consequences. Our results indicate that fine-scale snow albedo effects influence the response of both hot and cold events and that peak increases in extreme hot events are amplified by surface moisture feedbacks. Likewise, we find that extreme precipitation is enhanced on the lee side of rain shadows and over coastal areas dominated by convective precipitation. We project substantial, spatially heterogeneous increases in both hot and wet events over the contiguous United States by the end of the next century, suggesting that consideration of fine-scale processes is critical for accurate assessment of local- and regional-scale vulnerability to climate change.**

extreme climate | RegCM3 | regional climate model | United States | $CO_2$

Global concentrations of non-water-vapor greenhouse gases have increased exponentially since the industrial revolution (1). Experiments using coupled atmosphere–ocean general circulation models (GCMs) consistently reveal that continued increases in anthropogenic emissions of greenhouse gases will result in warming of Earth's surface (1, 2). Although the exact changes that this warming might cause in the coupled climate system are not completely understood, numerical experiments suggest that such warming will result in climate changes over a range of spatial and temporal scales (1).

Of particular interest is the potential response of extreme temperature and precipitation events (e.g., refs. 3–7). Such events exert critical controls on both human and natural systems, causing catastrophic losses of property (8) and human life (9), regulating the spread of invasive species (10) and exotic diseases (11, 12), and acting as a direct agent of species extinction (13). Future changes in extreme climate regimes could thereby have dramatic ecological, economic and sociological impacts.

Here, we focus on potential future changes in extreme temperature and precipitation events over the contiguous United States. Extreme events have had tremendous impact on the United States in recent years, including insured property losses in excess of $5 billion per year during the 1990s (14). Three events, the midwest drought in 1988–1989, Hurricane Andrew in 1992, and the midwest flood in 1993, accounted for $88 billion in total losses (14), and heat-waves in the summer of 1995 claimed 1,100 lives (14), including 525 in Chicago during a single 3-week period (15). In addition to these recent catastrophes, the late 20th century has exhibited positive trends in frequency of hot events (16) and heavy precipitation events (17, 18), and negative trends in frequency of cold events (16, 19). However, it is not clear whether these late-20th-century changes were anthropogenic or were the result of nonanthropogenic climate variability, in part because preceding 20th-century periods showed opposite trends in extreme temperature and precipitation (16, 17) and in part because the late 19th century exhibited similar positive trends in heavy precipitation (17).

Although anthropogenic enhancement of the global greenhouse effect is likely to alter the large-scale environment in which extreme events occur (20), it is not currently clear in what ways fine-scale feedbacks, such as through soil moisture and snow albedo, will modulate the regional and local responses to those large-scale changes. Therefore, to capture these fine-scale processes, we have used a regional climate model (RCM) to simulate the climate of the contiguous United States at very fine horizontal resolution. To the best of our knowledge, this multidecadal experiment at least doubles both the resolution and integration length of previous high-resolution simulations of future climate over the full contiguous United States (21–23). In applying state-of-the-science grid resolution, domain extent, and integration length, we hope to gain a more complete understanding of the sensitivity of extreme climate events to increases in anthropogenic emissions of greenhouse gases.

## Models and Methods

**Model Description.** We have applied the Abdus Salam Institute for Theoretical Physics Regional Climate Model, Version 3 (RegCM3) (24–26). The RegCM3 grid was centered at 39.00°N and 100.00°W and consisted of 145 points in the latitude direction and 220 points in the longitude direction. Grid points were separated at 25-km horizontal resolution with 18 levels in the vertical. The Lambert Conformal projection placed the grid corners at 49.20°N, 140.06°W (northwest); 49.09°N, 59.63°W (northeast); 19.53°N, 124.69°W (southwest); and 19.48°N, 75.13°W (southeast). Atmospheric boundary conditions for the RegCM3 integrations were provided by the National Aeronautics and Space Administration (NASA) Finite Volume General Circulation Model (FV-GCM) (27), which was run at 1° latitude × 1.25° longitude horizontal resolution with 18 levels in the vertical. Projected future sea surface temperatures (SSTs) were calculated by using the Hadley Centre HadCM3 coupled atmosphere–ocean GCM (28).

**Experimental Design.** We have performed two model integrations. The reference integration (*RF*) covered the period 1961 through 1985. Annual time-varying concentrations of atmospheric carbon dioxide ($CO_2$) for *RF* and the corresponding FV-GCM integration were taken from Schlesinger and Malyshev (29). Monthly time-varying SSTs were supplied by the Hadley Centre observed SST data set (30). The future integration (*A2*) covered the period 2071–2095. Annual time-varying atmospheric $CO_2$ values for *A2* and the corresponding FV-GCM integration were taken from years 2071–2095 of the Special Report on Emissions Scenarios A2 scenario (31). Monthly time-varying SSTs were created by using SST fields calculated by HadCM3, with differences in values between the HadCM3 A2 and reference simulations added to the HadSST observational data set, as described in Giorgi *et al.* (32).

RegCM3 was allowed to equilibrate by running the initial year

This paper was submitted directly (Track II) to the PNAS office.

Abbreviations: RCM, regional climate model; GCM, general circulation model; FV-GCM, finite volume GCM; SST, sea surface temperature; JJA, June–July–August; RegCM3, Abdus Salam Institute for Theoretical Physics Regional Climate Model, Version 3.

†To whom correspondence should be addressed. E-mail: diffenbaugh@purdue.edu.

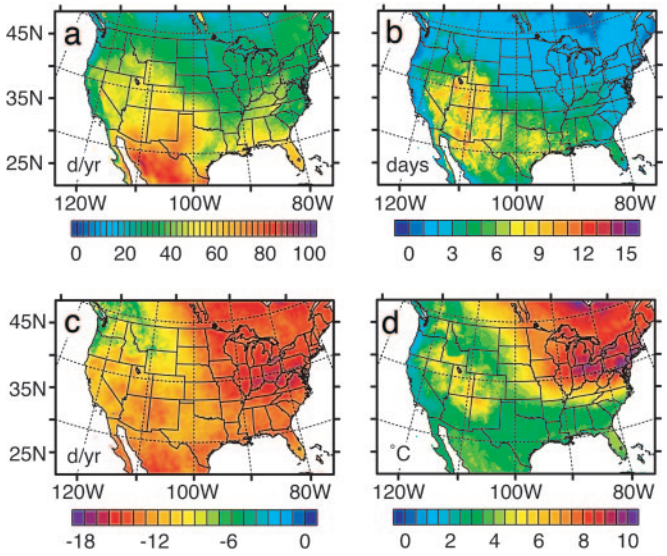


**Fig. 1.** Anomalies (*A2* − *RF*) in $T_{95}$ event frequency (days/year) (*a*), $T_{95}$ mean heat-wave length (days/event) (*b*), $T_{05}$ event frequency (days/year) (*c*), and 95th-percentile cold-event value (°C) (*d*). Only values for land and lake grid points that are statistically significant at the 95% confidence level are shown.

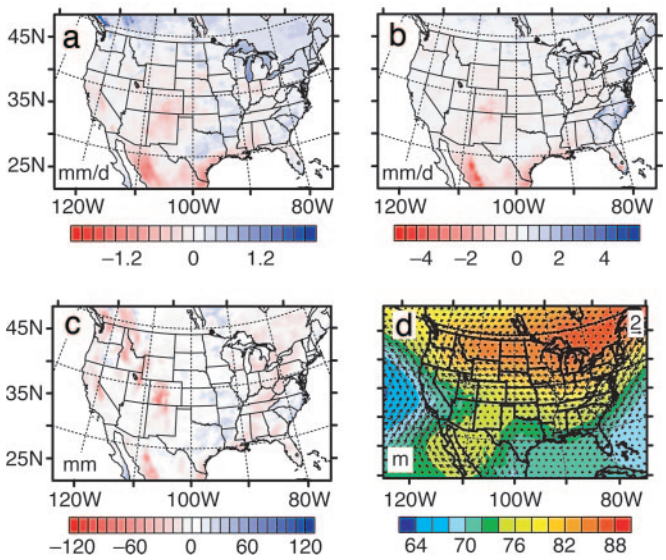


**Fig. 2.** Summer (JJA) anomalies (*A2* − *RF*) in evapotranspiration (mm/day) (*a*), total precipitation (*b*), root zone soil moisture (mm) (*c*), and 500-hPa heights (Pa) and winds (m/s) (*d*).

of each RegCM3 integration (1961 and 2071, respectively) twice, with the results of the first iterations used as initial conditions for the respective 25-year integrations analyzed here.

**Analysis of Extreme Events.** We analyzed daily maximum temperature, daily minimum temperature, and daily total precipitation from the *RF* and *A2* integrations. The $T_{95}$ ($T_{05}$) index value was calculated following Bell *et al.* (5) as the mean of the 95th percentile daily temperature maxima (5th percentile daily temperature minima) at each grid point in each of the 25 years of the *RF* integration. Mean heat-wave length was calculated following Diffenbaugh (33) as the number of consecutive days at each grid point in which the daily maximum temperature met or exceeded the corresponding grid-point $T_{95}$ index value. The mean annual 95th percentile extreme cold event was calculated as the mean of the 5th percentile daily temperature minima in each of the 25 years of the respective RCM integrations.

Following Salinger and Griffiths (34), rain-days were defined as days in which the total daily precipitation was ≥1.0 mm. The $P_{95}$ index value was defined following Bell *et al.* (5) at each grid point as the mean of the 95th percentile total precipitation values for the rain-days in each of the 25 years of the *RF* integration. Extreme precipitation contribution was calculated at each grid point as the fraction of total annual precipitation that fell during days in which total precipitation was greater than or equal to the corresponding grid-point $P_{95}$ index value. Dry days were defined as days in which total precipitation was less than or equal to the 1.0-mm threshold set by Salinger and Griffiths (34).

Differences in values between the *RF* and *A2* integrations were tested for statistical significance by using Student's *t* test. In these analyses, a buffer of eight grid points was discarded from each side of the RegCM3 domain to account for discontinuities in the FV-GCM/RegCM3 coupling.

## Results

**Extreme Temperature Events.** Anomalies (*A2* − *RF*) in extreme hot and cold events were statistically significant throughout the domain (Fig. 1). Anomalies in $T_{95}$ event frequency were positive, with peak changes of up to 100 days/year (560%) occurring over the southwestern United States and northern Mexico (Fig. 1*a*). Regional maxima occurred over the high-elevation areas of California (up to 400%), central Utah (up to 400%), central Idaho (up to 300%), the coast of mainland British Columbia (up to 200%), and the Appalachian Mountains (up to 280%). It is notable that even the minimum anomalies, which occurred along the coast of the Pacific Northwest and over southern Canada, represented a doubling of extreme hot-event frequency.

Anomalies in mean heat-wave length were also positive (Fig. 1*b*). Peak values of up to 15 days per event (up to 550%) stretched from northern Mexico into the northern Great Basin (Fig. 1*b*), with substantial spatial variability linked to the rugged terrain of the Great Basin. The northeast Atlantic coast, which showed strong positive anomalies in hot event frequency (Fig. 1*a*), showed little response in mean heat-wave length, whereas eastern Texas, which showed a minimum in the response of extreme hot-event frequency, showed a strong response in mean heat-wave length.

Anomalies in $T_{05}$ event frequency were negative throughout the domain, with peak anomalies of up to −17.5 days/year (up to −90%) occurring over low-elevation areas (Fig. 1*c*). The largest negative anomalies represented the near disappearance of $T_{05}$ events in the *A2* scenario. This change in the extreme cold regime was reflected in the substantial changes in temperature of the 95th-percentile cold event, which was up to 10°C warmer in the *A2* integration than in the *RF* integration (Fig. 1*d*).

A suite of climate system feedbacks modulated the response of extreme temperature events to the direct radiative effects of increased atmospheric greenhouse gas concentrations. For instance, the pattern of hot-event anomalies (Fig. 1 *a* and *b*) appears to have been caused in part by summer surface-moisture feedbacks in the *A2* integration. June–July–August (JJA) evapotranspiration anomalies (*A2* − *RF*) were negative over the southwestern United States and northern Mexico (Fig. 2*a*), amplifying direct radiative heating by decreasing latent cooling over these areas. Conversely, JJA evapotranspiration anomalies were positive over the central United States, the eastern seaboard, and southern Canada, muting direct radiative heating by increasing latent cooling. The anomalies in JJA evapotranspiration were closely associated with anomalies in JJA precipitation (Fig. 2*b*) and JJA soil moisture (Fig. 2*c*).

These fine-scale surface-moisture effects likely interacted with larger-scale climate processes. For instance, geopotential heights and anticyclonic flow were both enhanced at 500 hPa over the southwest United States and northern Mexico in the *A2* integration

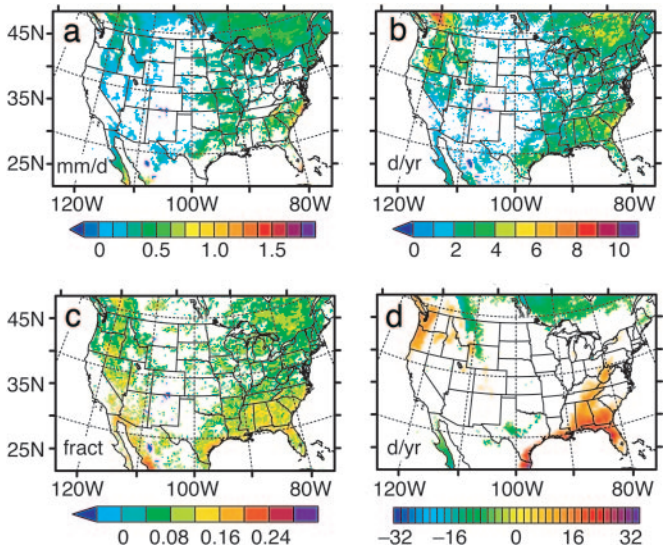


**Fig. 3.** Anomalies (*A2* − *RF*) in mean annual precipitation (mm/day) (*a*), $P_{95}$ event frequency (days/year) (*b*), extreme-precipitation fraction (fraction) (*c*), and dry-day frequency (days/year) (*d*). Only values for land and lake grid points that are statistically significant at the 95% confidence level are shown.

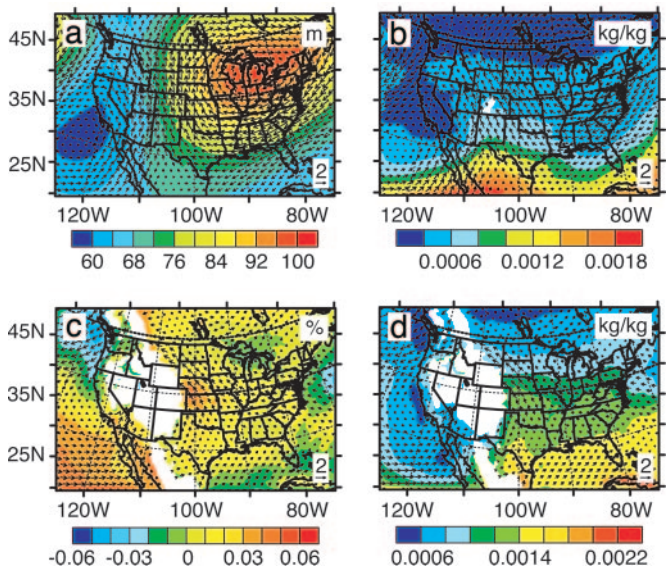


**Fig. 4.** Anomalies (*A2* − *RF*) in November–December–January 500-hPa heights (m) and winds (m/s) (*a*), November–December–January 700 hPa mixing ratio (kg/kg) and winds (m/s) (*b*), March–April–May 850-hPa relative humidity (%) and winds (m/s) (*c*), and March–April–May 850-hPa mixing ratio (kg/kg) and winds (m/s) (*d*).

(relative to the *RF* integration) (Fig. 2*d*). Although such changes aloft could have initiated the precipitation–soil moisture–evapotranspiration enhancement of extreme hot events by increasing surface temperatures and reducing clouds and precipitation, it is also possible that the larger-scale changes resulted from the changes in surface moisture balance (35). Although further study is required to ascertain the full nature of these multiscale climate system interactions, this experiment indicates that such interactions could exert critical controls on the response of extreme temperature events to anthropogenically elevated greenhouse-gas concentrations, particularly in arid regions.

The extreme temperature response also was regulated by land surface heterogeneity, including complexity of land cover and topography. For instance, the spatial variability of the summer soil-moisture anomalies in the western United States (Fig. 2*c*) was largely associated with the spatial variability of the land-cover boundary condition, which in the western United States closely follows the spatial variability of the topography. Additionally, the large positive anomalies in extreme hot events over the high elevations of California and southwestern Canada were associated with reductions in late spring and early summer snow cover in the *A2* integration (data not shown), indicating a positive snow albedo feedback linked to changes in the elevation of the freeze/melt transition. Similarly, in northern California (north of 40°N) and south-central Oregon (west of 120°W), reductions in extreme cold events were likely amplified by snow albedo feedbacks, with the largest anomalies in extreme cold events occurring in areas where substantial cold season snow cover was present in the *RF* integration but absent in the *A2* integration. Conversely, the response of cold extremes was muted in areas where snow cover persisted in the *A2* integration, with apparent snow mitigation of cold season warming in central Idaho, western Wyoming, and southwestern Canada. Because both the land cover and topography of the western United States vary at even smaller spatial scales than are represented here, further influence of these fine-scale climate feedbacks could be seen with greater increases in RCM spatial resolution.

**Extreme Precipitation Events.** Statistical significance of anomalies (*A2* − *RF*) in extreme precipitation varied across the domain (Fig. 3). Statistically significant anomalies in mean annual precipitation were almost entirely positive, with peak differences of up to 1.75 mm/day (up to 40%) over the mid-Atlantic coast (Fig. 3*a*). The patterns of statistically significant anomalies in extreme precipitation event frequency and contribution were very similar to those of mean annual precipitation (Fig. 3 *b* and *c*), including peak anomalies in extreme precipitation event frequency of up to 10 days/year (up to 140%) over the Pacific Northwest (Fig. 3*b*). The pattern of precipitation anomalies suggests a weakening of the orographic rain shadows in the Mountain West, due in large part to the changes in the extreme precipitation regime. For instance, positive anomalies in mean annual precipitation on the lee side of high elevations in southwestern Canada (near 120°W), eastern Washington, eastern Oregon, Nevada, and eastern Idaho were associated with large changes in extreme-event frequency and contribution (Fig. 3 *b* and *c*). Alternatively, over the Rocky Mountain rain shadows in southwestern Canada (just west of 110°W), central Montana, and central Wyoming, positive anomalies in mean annual precipitation were associated with negative changes in the frequency of dry days (up to −26 days/year, or −12%) (Fig. 3*d*). In either case, rain shadow weakening could have resulted from greenhouse-related increases in the moisture content of air being carried across mountain ranges [an extension of the conceptual model of Trenberth (36)] or from increases in upslope flow on the lee side of those ranges.

Many coastal areas also exhibited substantial increases in extreme event contribution, with peak positive anomalies of up to 0.28 (up to 110%) occurring over the west coast of northern Mexico (Fig. 3*c*). Over the Pacific Northwest and Gulf Coast regions, increases in extreme-event contribution were accompanied by increases in the frequency of dry days (Fig. 3*d*). Particularly in the case of the Gulf Coast, which exhibited substantial increases in mean annual precipitation and extreme precipitation frequency, the increases in dry-day frequency highlight the possibility that anthropogenic increases in greenhouse-gas concentrations could result in simultaneous enhancement of both wet and dry conditions.

The changes in extreme precipitation over the Pacific Northwest (Fig. 3) were related to changes in large-scale atmospheric flow during late autumn and winter (Fig. 4*a*). For this region, November–December–January is the period of climatological maximum precipitation (37), as well as the period of maximum positive anomalies (*A2* − *RF*) in extreme-event frequency in this experiment

**Table 1. Summary of selected extreme event responses**

| Response by region | Late 20th century trend? (ref.) | Primary mechanism(s) | Secondary mechanism(s) |
|---|---|---|---|
| Northwest | | | |
| Increased frequency of extreme hot events | Yes (16) | Radiative forcing | Snow albedo feedbacks |
| Decreased frequency of extreme cold events; less severe cold events | Equivocal (16) | Radiative forcing | Snow albedo feedbacks |
| Increased frequency and contribution of extreme precipitation events; weaker rain shadows | Yes (17, 18, 37) | Enhanced cyclonic flow aloft | Enhanced atmospheric moisture content |
| Northeast | | | |
| Increased frequency of extreme hot events | Yes (16) | Radiative forcing | — |
| Decreased frequency of extreme cold events; less severe cold events | Yes (16) | Radiative forcing | — |
| Southwest | | | |
| Increased frequency of extreme hot events; longer heat-waves | Yes (16) | Radiative forcing | Surface moisture feedbacks; enhanced anticyclonic flow aloft |
| Increased contribution of extreme precipitation events | Yes (37) | Enhanced low- and upper-level cyclonic flow | Enhanced atmospheric moisture content |
| Southeast | | | |
| Increased frequency of extreme hot events | Yes (16) | Radiative forcing | — |
| Decreased frequency of extreme cold events; less severe cold events | Yes (16) | Radiative forcing | — |
| Increased frequency and contribution of extreme precipitation events | Yes (17, 37) | Enhanced convective available potential energy | Enhanced coastal moisture convergence |

(data not shown). During November–December–January, the *A2* integration exhibited enhanced cyclonic flow and corresponding weak 500-hPa height increases off the west coast of the United States (Fig. 4*a*). This anomaly is consistent with that shown by Leung and Ghan (38) for December–January–February and, when coupled with positive anomalies in tropospheric moisture (Fig. 4*b*), suggests enhanced forcing of synoptic-scale ascent and hence clouds and precipitation. These mean wet-season changes in the *A2* integration indicate an atmospheric environment more likely to produce extreme daily precipitation.

Changes in precipitation extremes in the southeastern United States appeared to have been related less to large-scale dynamics, which exhibited only slight changes over that region (data not shown). Rather, extreme-event anomalies were associated with positive anomalies in lower-tropospheric moisture along the Gulf Coast in March–April–May (Fig. 4 *c* and *d*). Such increases in moisture content can contribute to increases in convective available potential energy and therefore to enhanced convective precipitation. Increases in atmospheric moisture associated with warmer Gulf of Mexico SSTs also likely increased coastal moisture convergence. Similar coastal SST effects likely contributed to the strong positive anomalies in extreme event contribution along the east coast of the Gulf of California, where peak positive anomalies in spring 850-hPa moisture content (Fig. 4*c*) and enhanced cyclonic flow at 850 hPa (Fig. 4*c*) and 500 hPa (data not shown) indicate increased transport of moisture against the topographic barrier of the Sierra Madre.

## Discussion

Key results of this study are summarized in Table 1. The changes in extreme temperature and precipitation events that we have projected in conjunction with future increases in atmospheric concentrations of greenhouse gases agree with the direction of change observed in the late-20th-century instrumental record. For example, our findings of positive changes (*A2* − *RF*) in extreme hot events and negative changes in extreme cold events (Fig. 1) are consistent with positive trends in extreme maximum temperatures and negative trends in extreme cold temperatures over the contiguous United States (16). Additionally, our finding of positive anomalies in extreme precipitation-event frequency and contribution is consistent with positive late-20th-century national trends (17, 39, 40). Further, the spatial pattern of 21st-century anomalies reported here is consistent with the spatial pattern in those late-20th-century trends (16–18). Although agreements between observed and projected changes in extreme climate regime do not directly attribute the late-20th-century trends to anthropogenic emissions of greenhouse gases, they do suggest that such trends could continue through the 21st century if greenhouse gas concentrations continue to rise at their current rates.

The changes in frequency and magnitude of extreme temperature and precipitation events projected here could have dramatic impacts on human and natural systems. For instance, agricultural production (41–44), water storage (45–48), seasonal energy demands, catastrophic flood loss (8), and human mortality (9) could all be substantially affected. Further, natural ecosystems could be severely impacted through changes in plant community composition and biogeography (49, 50) and increases in risks of extinction (13), invasion (10), and exotic disease (12).

Although we have devoted substantial computational resources to maximizing the RCM grid resolution, domain size, and integration length, there are potentially important climate processes that we have not considered. For instance, still-longer RCM integrations will allow for investigation of the dynamics controlling extreme events of longer return period, including rare precipitation events (18). Additionally, we have not included equilibrium climate-vegetation feedbacks or projections of future human land use change, both of which could modulate the response of extreme temperature and precipitation events to anthropogenic changes in greenhouse forcing (33, 51). Nor have we considered regional-scale atmosphere–ocean feedbacks, which could influence both regional- and large-scale climate processes (52). Further, we have neglected transient changes in aerosol concentrations, which could contribute substantially to changes in cloud microphysics and net radiative forcing (1).

## Conclusions

We have tested the response of extreme temperature and precipitation events over the contiguous United States to the Special

Report on Emissions Scenarios A2 emissions scenario using an RCM configuration that doubles the resolution and integration length of previous high-resolution climate-change experiments. In response to increases in atmospheric concentrations of greenhouse gases, the frequency and magnitude of extreme events changes dramatically, with increases in extreme hot events, decreases in extreme cold events, and increases in extreme precipitation events.

Our results indicate that, should atmospheric greenhouse gas concentrations continue to increase over the next century, changes in the frequency and magnitude of extreme events are likely to be dictated not only by changes in large-scale climate dynamics but also by a suite of climate-system modifiers operating at very fine scales. For instance, we found that, in topographically complex terrain, spatially heterogeneous changes in snow cover exerted albedo feedbacks on both extreme hot and extreme cold events. Similarly, the persistence of snow cover likely mitigated changes in the frequency and magnitude of extreme cold events, creating areas of high spatial variability in cold-season sensitivity to anthropogenic emissions of greenhouse gases. Further, extreme hot events were both amplified and muted by surface-moisture effects that appeared to have resulted from complex, two-way interactions between large-scale atmospheric circulation and fine-scale spatial variability in topography, natural land cover, and human land use. Fine-scale processes also played a critical role in the response of extreme precipitation events, with changes in large-scale circulation intensifying wet-season storms but increasing extreme-event frequency only on the lee side of Pacific coast rain shadows. Further, coastal processes related to tropospheric moisture content likely played a critical role in the areas of the southeastern United States and northern Mexico that exhibited a large response of extreme-precipitation contribution.

Our results illustrate that important climate-system modifiers operate at very fine scales and that each can substantially influence local changes in extreme temperature and precipitation events. These fine-scale processes also can interact with large-scale dynamics to dramatically amplify or mute the primary effects of anthropogenically enhanced greenhouse forcing. Because of their potential influence on local and extra-local climate dynamics, consideration of these fine-scale processes is critical for accurate assessment of the possible impacts of global warming on natural and human systems.

We thank two anonymous reviewers for their insightful and constructive comments. We thank F. Kucharski and X. Bi for access to the FV-GCM simulations and H. Bae for assistance in porting RegCM3 to the computational facilities in the Rosen Center for Advanced Computing, which are supported and administered by Information Technology at Purdue. We thank the Abdus Salam International Centre for Theoretical Physics for support of and access to RegCM3 and the Hadley Center for providing the HadCM3 SST data and the HadSST data set. This work was partly supported by National Science Foundation Award 0315677. This work is Purdue Climate Change Research Center paper no. 0516.

1. Intergovernmental Panel on Climate Change, W. G. I. (2001) *Climate Change 2001: The Scientific Basis* (Cambridge Univ. Press, New York).
2. Meehl, G. A., Washington, W. M., Collins, W. D., Arblaster, J. M., Hu, A. X., Buja, L. E., Strand, W. G. & Teng, H. Y. (2005) *Science* **307,** 1769–1772.
3. Zwiers, F. W. & Kharin, V. V. (1998) *J. Climate* **11,** 2200–2222.
4. Kharin, V. V. & Zwiers, F. W. (2000) *J. Climate* **13,** 3760–3788.
5. Bell, J. L., Sloan, L. C. & Snyder, M. A. (2004) *J. Climate* **17,** 81–87.
6. Pal, J. S., Giorgi, F. & Bi, X. Q. (2004) *Geophys. Res. Lett.* **31,** L13202, 10.1029/2004GL019836.
7. Christensen, J. H. & Christensen, O. B. (2003) *Nature* **421,** 805–806.
8. Easterling, D. R., Meehl, G. A., Parmesan, C., Changnon, S. A., Karl, T. R. & Mearns, L. O. (2000) *Science* **289,** 2068–2074.
9. Kalkstein, L. S. & Greene, J. S. (1997) *Environ. Health Perspect.* **105,** 84–93.
10. Walther, G. R., Post, E., Convey, P., Menzel, A., Parmesan, C., Beebee, T. J. C., Fromentin, J. M., Hoegh-Guldberg, O. & Bairlein, F. (2002) *Nature* **416,** 389–395.
11. DeGaetano, A. T. (2005) *Int. J. Biometeorol.* **49,** 345–353.
12. Marra, P. P., Griffing, S., Caffrey, C., Kilpatrick, A. M., McLean, R., Brand, C., Saito, E., Dupuis, A. P., Kramer, L. & Novak, R. (2004) *Bioscience* **54,** 393–402.
13. Parmesan, C., Root, T. L. & Willig, M. R. (2000) *Bull. Am. Meteorol. Soc.* **81,** 443–450.
14. Changnon, S. A., Pielke, R. A., Changnon, D., Sylves, R. T. & Pulwarty, R. (2000) *Bull. Am. Meteorol. Soc.* **81,** 437–442.
15. Changnon, S. A., Kunkel, K. E. & Reinke, B. C. (1996) *Bull. Am. Meteorol. Soc.* **77,** 1497–1506.
16. DeGaetano, A. T. & Allen, R. J. (2002) *J. Climate* **15,** 3188–3205.
17. Kunkel, K. E., Easterling, D. R., Redmond, K. & Hubbard, K. (2003) *Geophys. Res. Lett.* **30,** 1900, 10.1029/2003GL018052.
18. Groisman, P. Y., Knight, R. W., Easterling, D. R., Karl, T. R., Hegerl, G. C. & Razuvaev, V. A. N. (2005) *J. Climate* **18,** 1326–1350.
19. Kunkel, K. E., Easterling, D. R., Hubbard, K. & Redmond, K. (2004) *Geophys. Res. Lett.* **31,** L03201, 10.1029/2003GL018624.
20. Meehl, G. A. & Tebaldi, C. (2004) *Science* **305,** 994–997.
21. Pan, Z. T., Arritt, R. W., Takle, E. S., Gutowski, W. J., Anderson, C. J. & Segal, M. (2004) *Geophys. Res. Lett.* **31,** L17109, 10.1029/2004GL020528.
22. Chen, M., Pollard, D. & Barron, E. J. (2003) *J. Geophys. Res. Atmos.* **108,** 4348, 10.1029/2002JD002738.
23. Leung, L. R., Qian, Y., Bian, X. D., Washington, W. M., Han, J. G. & Roads, J. O. (2004) *Climatic Change* **62,** 75–113.
24. Giorgi, F., Marinucci, M. R. & Bates, G. T. (1993) *Monthly Weather Rev.* **121,** 2794–2813.
25. Giorgi, F., Marinucci, M. R., Bates, G. T. & Decanio, G. (1993) *Monthly Weather Rev.* **121,** 2814–2832.
26. Pal, J. S., Small, E. E. & Eltahir, E. A. B. (2000) *J. Geophys. Res. Atmos.* **105,** 29579–29594.
27. Atlas, R., Reale, O., Shen, B. W., Lin, S. J., Chern, J. D., Putman, W., Lee, T., Yeh, K. S., Bosilovich, M. & Radakovich, J. (2005) *Geophys. Res. Lett.* **32,** L03807, 10.1029/2004GL021513.
28. Johns, T. C., Gregory, J. M., Ingram, W. J., Johnson, C. E., Jones, A., Lowe, J. A., Mitchell, J. F. B., Roberts, D. L., Sexton, D. M. H., Stevenson, D. S., *et al.* (2003) *Climate Dyn.* **20,** 583–612.
29. Schlesinger, M. E. & Malyshev, S. (2001) *Integrated Assessment* **2,** 95–199.
30. Rayner, N. A., Parker, D. E., Horton, E. B., Folland, C. K., Alexander, L. V., Rowell, D. P., Kent, E. C. & Kaplan, A. (2003) *J. Geophys. Res. Atmos.* **108,** 4407, 10.1029/2002JD002670.
31. Intergovernmental Panel on Climate Change, W. G. I. (2000) *Special Report on Emissions Scenarios* (Cambridge Univ. Press, Cambridge, U.K.).
32. Giorgi, F., Bi, X. & Pal, J. S. (2004) *Climate Dyn.* **22,** 733–756.
33. Diffenbaugh, N. S. (2005) *Geophys. Res. Lett.* **32,** L07702, 10.1029/2004GL022184.
34. Salinger, M. J. & Griffiths, G. M. (2001) *Int. J. Climatol.* **21,** 1437–1452.
35. Pal, J. S. & Eltahir, E. A. B. (2003) *Q. J. Royal Meteorol. Soc.* **129,** 2279–2297.
36. Trenberth, K. E. (1999) *Climatic Change* **42,** 327–339.
37. Mock, C. J. (1996) *J. Climate* **9,** 1111–1125.
38. Leung, L. R. & Ghan, S. J. (1999) *J. Climate* **12,** 2031–2053.
39. Karl, T. R. & Knight, R. W. (1998) *Bull. Am. Meteorol. Soc.* **79,** 231–241.
40. Groisman, P. Y., Knight, R. W., Karl, T. R., Easterling, D. R., Sun, B. & Lawrimore, J. M. (2004) *J. Hydrometeorol.* **5,** 64–85.
41. Linden, L. (2001) *Can. J. Plant Sci.* **81,** 479–485.
42. Caprio, J. M. & Quamme, H. A. (1999) *Can. J. Plant Sci.* **79,** 129–137.
43. Wilhelm, E. P., Mullen, R. E., Keeling, P. L. & Singletary, G. W. (1999) *Crop Sci.* **39,** 1733–1741.
44. Ferris, R., Ellis, R. H., Wheeler, T. R. & Hadley, P. (1998) *Ann. Botany* **82,** 631–639.
45. Johnk, K. D., Straile, D. & Ostendorp, W. (2004) *Limnologica* **34,** 15–21.
46. Thompson, S. M. (2003) *J. Hydrol. Eng.* **8,** 190–196.
47. Malek, E. (2003) *Int. J. Climatol.* **23,** 333–345.
48. Tereshchenko, I., Filonov, A., Gallegos, A., Monzon, C. & Rodriguez, R. (2002) *J. Hydrol.* **264,** 133–146.
49. Gurvich, D. E., Diaz, S., Falczuk, V., Perez-Harguindeguy, N., Cabido, M. & Thorpe, P. C. (2002) *Global Change Biol.* **8,** 1139–1145.
50. Penuelas, J., Filella, I., Zhang, X. Y., Llorens, L., Ogaya, R., Lloret, F., Comas, P., Estiarte, M. & Terradas, J. (2004) *New Phytol.* **161,** 837–846.
51. Zhao, M. & Pitman, A. J. (2002) *Geophys. Res. Lett.* **29,** 10.1029/2001JD000931.
52. Large, W. G. & Danabasoglu, G. (2005) *J. Climate*, in press.